

# A MODEL FOR X-RAY BRIGHT POINTS DUE TO UNEQUAL CANCELLING FLUX SOURCES

C. E. PARNELL, E. R. PRIEST

*Department of Mathematical and Computational Sciences, University of St. Andrews, St. Andrews  
KY16 9SS, Scotland*

and

V. S. TITOV

*Program Systems Institute of the Russian Academy of Sciences, 152140 Pereslavl-Zalessky, Russia*

(Received 29 January, 1994; in revised form 2 April, 1994)

**Abstract.** A recent discovery from the Big Bear Solar Observatory has linked the cancellation of opposite polarity magnetic fragments in the photosphere (i.e., so-called cancelling magnetic features) to X-ray bright points and has stimulated the setting up of a converging flux model for the process. Cancelling magnetic features can occur between magnetic fragments of differing strengths in many different situations. Here, therefore, we model two opposite polarity fragments of different strengths in the photosphere by two unequal sources in an overlying uniform field. Initially in the *pre-interaction phase* these sources are assumed to be unconnected, but as they move closer together the *interaction phase* starts with an X-type neutral point forming, initially on the photosphere, then rising up into the chromosphere and corona before lowering back down to the photosphere. The *capture phase* then follows with the sources fully connected as they move together. Finally, after they come in to contact, during the *cancellation phase* the weaker source is cancelled by part of the stronger source. The height of the X-type neutral point varies with the separation of the sources and the ratio of the source strengths, as do the positions of the neutral points before connection and after complete reconnection of the two sources. The neutral point is the location of magnetic reconnection and therefore energy release which is believed to power the X-ray bright point in the corona. By using a current sheet approximation, where it is assumed no reconnection takes place as the two sources move together, the total amount of energy released during reconnection may be estimated. The typical total free magnetic energy is found to be of the order of  $10^{20} - 10^{21}$  J, which is as required for an X-ray bright point. It is also found that, as the ratio of the source strengths increases, the height of the X-type neutral point decreases, as do the total energy released, and the lifetime of the bright point.

## 1. Introduction

The photosphere of the Sun is threaded by many intricate regions of positive and negative magnetic flux. Pairs of opposite polarity magnetic fragments, not necessarily of the same strengths, are often seen to cancel (Martin, 1984, 1986, 1988). Such an event is known as a cancelling magnetic feature. In order to try and explain such events and their accompanying X-ray bright points, a converging flux model has been set up by Priest, Parnell, and Martin (1994) including a detailed model for the interaction of two sources of the same strength, but opposite sign, situated in an overlying uniform field. In the converging flux model the magnetic fragments move through a series of potential states since the characteristic velocity is much smaller than the Alfvén velocity. The two sources are modeled by poles and are originally considered to be situated sufficiently far apart that their magnetic

*Solar Physics* **153**: 217–235, 1994.

© 1994 Kluwer Academic Publishers. Printed in Belgium.

fields are unconnected. This is known as the *pre-interaction phase*. As the sources move closer together they first come into contact when the sources have a half-separation of  $d$ , where  $d$  is known as the *interaction distance*. Here an X-type neutral point forms on the photosphere, and the *interaction phase* begins, during which the X-type neutral point rises into the chromosphere and corona as the two sources move closer, until at zero separation the *cancellation phase* starts and once again the neutral point is on the photosphere. The model accounts for many of the key observations of X-ray bright points and cancelling magnetic features. The pre-interaction phase has the sources unconnected and therefore implies no chromospheric fibrils joining the fragments. It explains how the X-ray bright point occurs before the cancelling magnetic feature, with reconnection in the lower corona during the interaction phase releasing energy, whilst reconnection in the photosphere during the cancellation phase causes the cancelling magnetic feature. In addition, when the reconnection point is passing through the upper chromosphere or low transition region and energy release is especially strong, it could give rise to the HRTS jets which Dere (1993) has described. Also the active-region transient brightenings (Shimizu *et al.*, 1992) and X-ray jets (Shibata *et al.*, 1992) observed by the YOHKOH satellite may well be created by the process modelled here. In fact, Shibata *et al.* have sketched a cartoon of what may be going on in an X-ray jet, which is qualitatively similar to the picture and detailed working we are presenting here.

To calculate the total amount of energy released during the reconnection, Priest, Parnell, and Martin (1994) conducted a thought experiment in which a current sheet is allowed to form as the sources move together. The free energy stored in the current sheet was calculated and found to be of the order  $10^{20} - 10^{21}$  J for two sources with an interaction distance of 5–10 Mm and situated in an ambient field of 10 G. This corresponds very well to the emission from a normal X-ray bright point lasting for 8 hr which would release a total energy of  $3 \times 10^{20} - 3 \times 10^{21}$  J.

Following on from their work a study has been carried out in this paper analysing in a similar way the interaction of two oppositely directed sources of different strengths in an overlying horizontal field. As in Priest, Parnell, and Martin (1994), the sources are initially assumed to evolve through a series of quasi-static states. Again the magnetic field structures have different topologies in the pre-interaction phase, the interaction phase and the cancellation phase, but here an extra phase occurs called the *capture phase*, which starts after the interaction phase and before the cancellation phase. These phases are all considered in Section 2, which also includes a study of the positions of the neutral points in the different phases as the positions and strengths of the sources vary. In Section 3 it is assumed that no reconnection takes place as the sources move together and so a current sheet forms extending up from the photosphere. The magnetic field due to the current sheet is calculated and the variation of the end-points of the current sheet as the sources move is studied. The current sheet approximation is used to estimate the total amount of energy released in the reconnection between the two sources.

## 2. Interaction of Two Unequal Sources in a Uniform Field

Magnetic fragments in the photosphere move at approximately  $0.5\text{--}1.0\text{ km s}^{-1}$ , a velocity much slower than the typical Alfvén velocity of  $1000\text{ km s}^{-1}$ , and so the interaction of these fragments may be considered to evolve through a series of quasi-static potential states. Consider two poles, one of strength  $-g$  situated at  $z = -a$  on the real axis of the complex plane and of the other of strength  $f$  positioned at  $z = a$ ; they represent two magnetic regions of opposite sign and differing strengths lying in the plane of photosphere. The  $y$ -axis corresponds to a vertical axis extending from the photosphere into the chromosphere and corona. We shall assume that there is a horizontal uniform magnetic field overlying these poles and produced by distant sources. Such a horizontal field is reasonable on both observational and theoretical grounds since  $H\alpha$  pictures of the chromosphere invariably show fibril structures crossing supergranule cells. In addition most of the photospheric magnetic flux is concentrated into strong magnetic field regions such as sunspots or intense flux tubes at supergranule boundaries, so that as this extends upwards it fans out to produce a predominantly horizontal structure, at least in the lower corona. The potential magnetic field for this situation can be written using complex variable theory in terms of the complex function  $\mathcal{B}_p(z)$ , where  $z = x + iy$ ,

$$\begin{aligned}\mathcal{B}_p(z) &= B_{py}(x, y) + iB_{px}(x, y) = \\ &= iB_0 + \frac{if}{\pi(z-a)} - \frac{ig}{\pi(z+a)} = \\ &= \frac{iB_0(z^2 + (f' - g')z + a(f' + g' - a))}{z^2 - a^2},\end{aligned}\quad (1)$$

where  $B_0$  is the strength of the ambient magnetic field,  $f' = f/(\pi B_0)$ ,  $g' = g/(\pi B_0)$ ,  $B_{px}(x, y)$ , and  $B_{py}(x, y)$  are the components of the potential magnetic field  $B_p(x, y)$  parallel and perpendicular to the plane of the photosphere, respectively, and  $a$  is the half-separation of the poles.

The position,  $z_n$ , of the neutral points can be found by determining where  $\mathcal{B}_p = 0$ , namely

$$z_n^2 + (f' - g')z_n + a(f' + g' - a) = 0, \quad (2)$$

which has solution

$$z_n = \frac{-(f' - g') \pm \sqrt{(f' - g')^2 - 4a(f' + g' - a)}}{2}. \quad (3)$$

When  $z_n$  is purely real and single-valued there will be a single neutral point which lies on the photosphere; this happens when

$$(f' - g')^2 - 4a(f' + g' - a) = 0,$$

which implies

$$a = \frac{f' + g'}{2} \pm \sqrt{f'g'}.$$

Let

$$d_i = (f' + g')/2 + \sqrt{f'g'} \quad (4)$$

be called the *interaction distance* and

$$d_c = (f' + g')/2 - \sqrt{f'g'} \quad (5)$$

be called the *capture distance*. When  $f = g$  (the particular case studied by Priest, Parnell, and Martin, 1994),  $d_c = 0$  and  $d_i$  reduces to the value  $2f'$  used by them. Initially, when the poles have a half-separation of  $a > d_i$  (the pre-interaction phase), they are unconnected and there are two neutral points given by Equation (3) on the photosphere (Figure 1(a)). Figure 2(a) shows how the two neutral points converge as the half-separation,  $a$  tends to  $d_i$ . As the poles move together they first come into contact when  $a = d_i$ , the interaction distance. When  $a = d_i$  (the start of the interaction phase) a neutral point forms on the  $x$ -axis at  $z_n = -(f' - g')/2$ , as shown in Figure 1(b). During the interaction phase the poles continue moving together and their half-separation,  $a$ , lies in the range  $d_c < a < d_i$ . Here  $z_n$  is given by

$$z_n = (x_n, y_n) = \left( \frac{-(f' - g')}{2}, \frac{+\sqrt{4a(f' + g' - a) - (f' - g')^2}}{2} \right) \quad (6)$$

and has both real and imaginary parts, so the X-type neutral point lies above the photosphere, as seen in Figure 1(c).

It is interesting to note that the neutral point does not move horizontally relative to the midpoint 0, between the two sources as the poles move from  $d_i$  to  $d_c$ , but it only moves vertically (Figure 2(b)). Instead, in the frame of the point 0, the weaker of the two poles is seen to move under the neutral point, so the X-ray bright point will not lie directly above the cancelling magnetic feature when it starts, but it will be located to one side as seen in Figure 1(c). A maximum height is gained by the X-type neutral point when  $dy_n/da = 0$ , which occurs when  $a = (f' + g')/2$ , and  $y_n = y_{n \max} = \sqrt{f'g'}$ , as shown in Figure 2(b). The neutral point then descends back down to the photosphere once more, where at  $a = d_c$ , the capture distance, the weaker pole becomes fully connected to the stronger pole (Figure 1(d)). As the two poles continue to move together reconnection ceases and the *capture phase* starts. With the weaker pole now fully connected to the stronger pole, two neutral points appear on the photosphere, lying to the left of the poles (Figure 1(e)). The

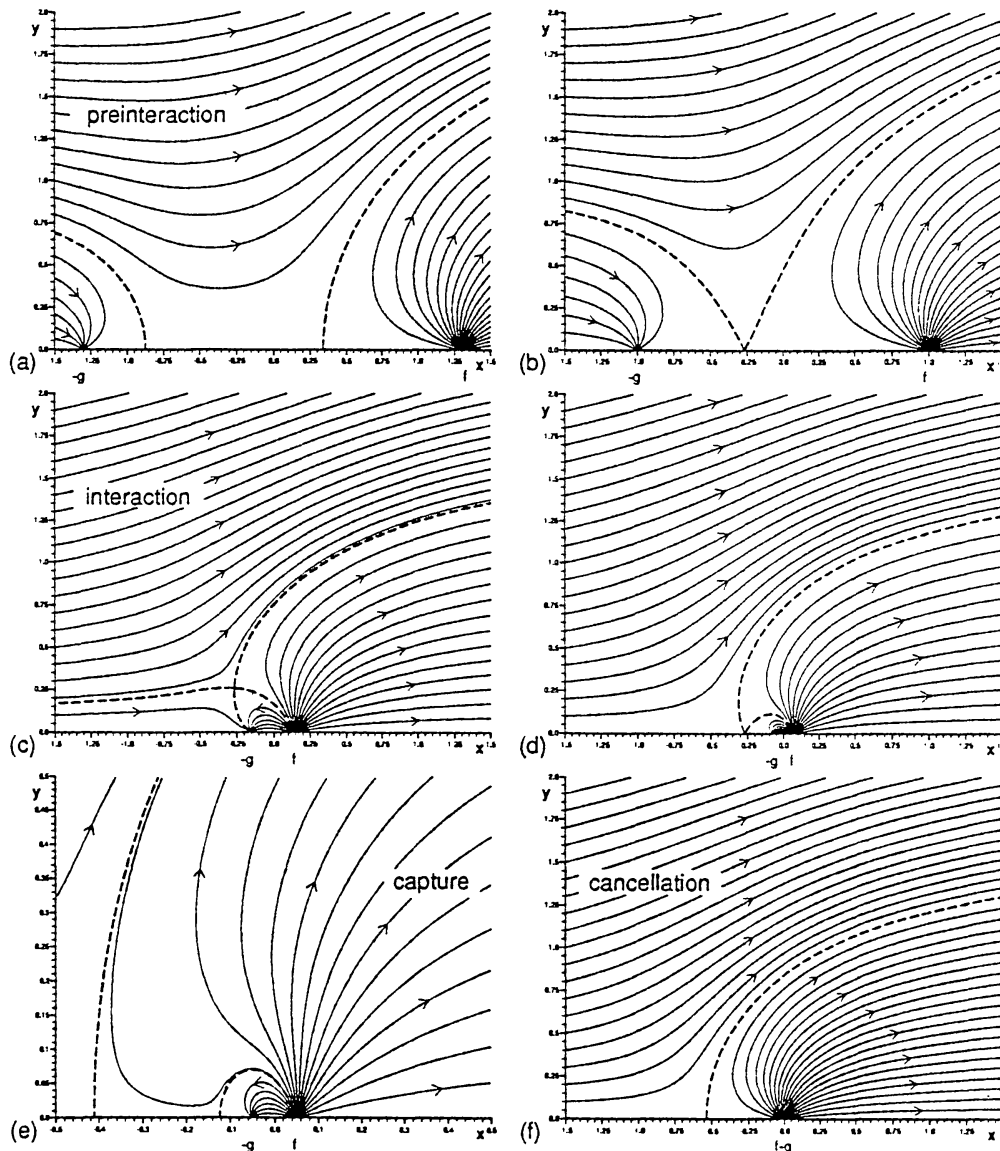


Fig. 1. The magnetic field due to two poles of strengths  $f (= 3g)$  and  $-g$ , positioned, respectively, at  $z = a$  and  $z = -a$  with a uniform background field of strength  $B_0 = 10$  G, where  $d_i$ , the interaction distance, is normalized to 1.0, and so  $g = \pi B_0 / (2 + \sqrt{3})$ . (a) The half-separation,  $a = 1.3$ , of the poles is greater than the interaction distance,  $d_i$  (the pre-interaction phase). (b)  $a = d_i$  and an X-type neutral point is formed. (c) When  $a = 0.15$  the X-type neutral point is positioned above the photosphere (during the interaction phase). (d) At  $a = d_c = (2 - \sqrt{3}) / (2 + \sqrt{3})$  the capture phase starts. The region showing the magnetic field is then enlarged in (e) where  $a = 0.05$  and pole  $-g$  is completely 'captured' by pole  $f$ . Zero separation of the poles in (f) shows the cancellation phase.

neutral points diverge until the poles have zero separation (Figure 2(c)), when at  $a = 0$ , in this model, the cancellation phase starts (Figure 1(f)).

The interaction distance,  $d_i$ , depends on the ratio of the strengths of the poles. If it is assumed that  $f = kg$ , where  $k$  is a constant ( $k > 0$ ),  $d_i$  and  $d_c$  can be written as

$$d_i = \left( \frac{k+1}{2} + \sqrt{k} \right) g' \quad (7)$$

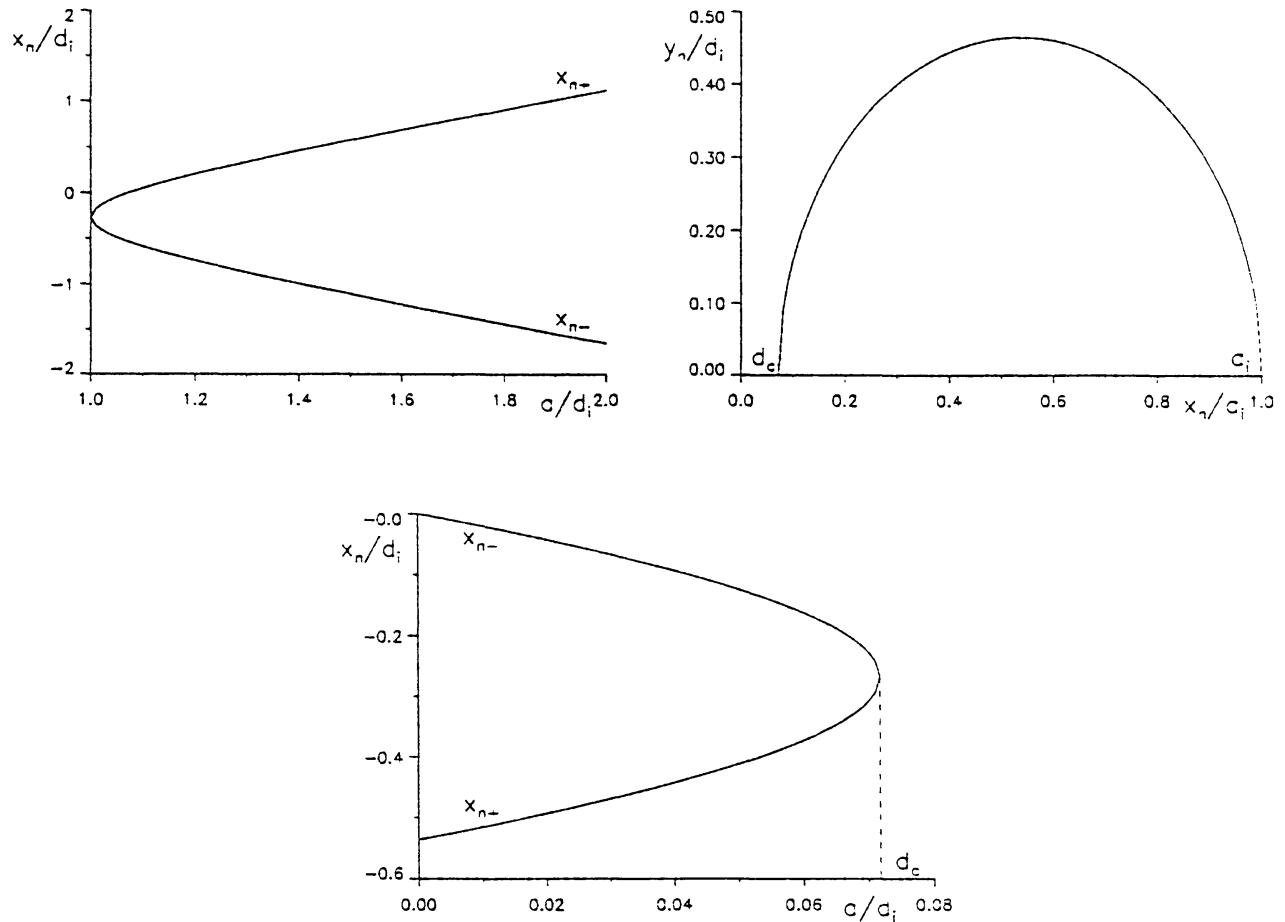


Fig. 2. (a) For poles  $f(=3g)$  and  $-g = -\pi B_0/(2 + \sqrt{3})$ , a graph of the positions of the neutral points,  $x_{n+}$  and  $x_{n-}$ , on the photosphere against the half-separation,  $a$ , when  $a$  is greater than the interaction distance  $d_i$ . (b) The height of the neutral point,  $y_n$ , above the photosphere is plotted versus the half-separation  $a$ , when  $d_c < a < d_i$ . (c) A graph of the positions of the neutral points,  $x_{n+}$  and  $x_{n-}$ , on the photosphere plotted against  $a$  which varies between 0.0 and  $d_c$ , the capture distance for the above poles.

and

$$d_c = \left( \frac{k+1}{2} - \sqrt{k} \right) g' . \quad (8)$$

If  $f$  is bigger than  $g$  (i.e.,  $k > 1$ ), then as  $k$  increases the interaction and capture distances increase. If  $g$  is bigger than  $f$  (i.e.,  $k < 1$ ), then as  $k$  decreases (i.e.,  $g$  becomes proportionally bigger) the interaction distance decreases but the capture distance increases (Figure 3(a)).

If the typical velocity of two interacting fragments is taken to be  $v$ , then the typical life time,  $t_L$ , for an X-ray bright point will be

$$t_L = \frac{d_i - d_c}{v} = \frac{2\sqrt{k} d_i}{((k+1)/2 + \sqrt{k})v} . \quad (9)$$

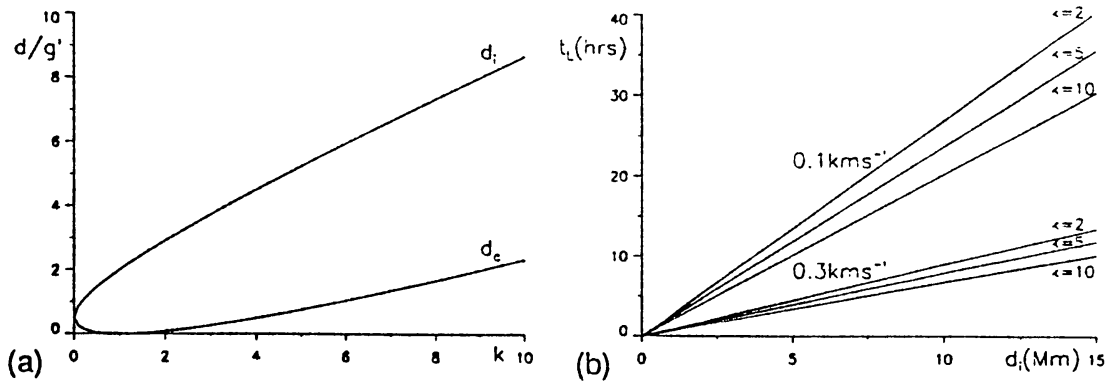


Fig. 3. (a) A graph of the values of the interactive distance ( $d_i$ ) and capture distance ( $d_c$ ) versus  $k = f/g$ , the pole strength ratio. (b) The predicted lifetimes ( $t_L$ ) for X-ray bright points versus the interaction distance ( $d_i$ ) when the velocities of interaction of the poles are  $0.3 \text{ km s}^{-1}$  and  $0.1 \text{ km s}^{-1}$  and the pole strength ratios ( $k$ ) are 2, 5, and 10.

For intracell/network cancellations,  $v$  is approximately  $0.3 \text{ km s}^{-1}$  and  $k$  is approximately 10, and so interaction distances of 2, 5, and 10 Mm, respectively, give the lifetimes ( $t_L$ ) for the bright points of 1.4, 3.4, and 6.8 hr, respectively. By comparison, the observed cancellation times are 1–5 hr. Ephemeral region/network or ephemeral region/intracell cancellations have velocities ( $v$ ) of approximately  $0.1\text{--}0.3 \text{ km s}^{-1}$  and  $k$  approximately 5, and so interaction distances of 2, 5, 10, and 15 Mm give lifetimes for the bright points of 5–2, 12–4, 24–8, 36–12 hr, respectively. Observed cancellation times are 1–36 hr. Network/network cancellations have  $v$  of approximately  $0.1\text{--}0.3 \text{ km s}^{-1}$  and  $k$  approximately 2, and so interaction distances of 5, 10, and 15 Mm produce lifetimes for the bright points of 14–5, 27–9, 40–14 hr, respectively (Figure 3(b)). Again 1–36 hr are the observed cancellation times. X-ray bright points are known to have lifetimes between 2–48 hr (Golub *et al.*, 1974), so from the lifetimes predicted by this model it is easy to see why such a great range could arise. If  $k$  is of order 1 and  $d_i$  large then the bright point will have a long lifetime, as in the network/network cancellations with  $d_i = 10\text{--}15$  Mm. If  $k$  is large and  $d_i$  small a short bright point lifetime ensues, as seen with intracell/network cancellations with  $d_i = 2\text{--}5$  Mm.

On the Sun the magnetic fragments that cancel to produce cancelling magnetic features have a non-zero width, so let us consider briefly a model with sources having a non-zero width  $2w$ , say, and suppose the half-separation ( $a$ ) is measured to the centre of the sources and cancellation begins when  $a = w$  (rather than  $a = 0$ ) when the sources come into contact. The capture phase will therefore only exist if  $d_c > w$ , so let us estimate their values. The typical width of intracell and network fields is 1–5 Mm, with respect to the present resolution, so cancellation will start at half-separations ( $w$ ) of around 2.5 Mm. In intracell/network cancellations  $k$  is approximately 10 and interaction distances of 2, 5, and 10 Mm give capture distances ( $d_c$ ) of 0.5, 1.3, and 2.7 Mm, respectively, using Equations (7) and (8). This implies that only those intracell fields with the largest interaction distances will

exhibit a capture phase after the bright point and before the cancelling magnetic feature. When a capture phase does occur, the height of the reconnected field lines will usually be relatively low, below the chromosphere, and so no fibrils would appear. For ephemeral regions the typical widths of fragments are 1–5 Mm as before. Ephemeral region/network or ephemeral region/intracell cancellations have pole strength ratios ( $k$ ) of approximately 5 and so interaction distances of 2, 5, 10, and 15 Mm, respectively, give capture distances of 0.3, 0.7, 1.5, and 2.2 Mm; therefore in these types of cancelling magnetic features a capture phase is unlikely to be seen other than in the situations where the sources start interacting at distances of more than 15 Mm. This implies that photospheric cancellation will probably start before the end of the X-ray bright point, as seen in most situations on the Sun. Network fields have sizes of 1–10 Mm, and therefore cancellation will start at half-separations of about 5 Mm. In network/network cancellations with  $k$  approximately 2 and interaction distances of 5, 10, and 15 Mm, the capture distances are found to be 0.15, 0.3, and 0.44 Mm, respectively, implying that a capture phase is very unlikely to occur, and the cancelling magnetic feature will probably start relatively soon into the life of the bright point.

Of course, magnetic fragments are unlikely to be of the same size in reality and so cancellation will not necessarily start right at the midpoint between the fragment centres. Also the magnetic fragments may well start to cancel before they actually come into contact as reconnection in the photosphere may cause some submergence, but the above considerations give explanations as to why cancelling magnetic features and X-ray bright points overlap in timing and give an idea as to which type of cancellation is most likely to give rise to a bright point before the cancellation itself starts.

The position of the X-type neutral point in the interaction phase can be written in terms of  $k$  and  $d_i$  as

$$x_n = \frac{-(\sqrt{k} - 1)d_i}{(\sqrt{k} + 1)}, \quad (10)$$

as can the maximum height of the X-type neutral point,

$$y_{n \max} = \frac{2\sqrt{k} d_i}{(\sqrt{k} + 1)^2}. \quad (11)$$

They are plotted in Figure 4(a), where it is found that, as the pole strength ratio ( $k$ ) increases, the position of the X-type neutral point in the interaction phase, and hence the bright point, moves further away from the midpoint of the sources. As the interaction distance increases, the neutral point also moves further from the midpoint of the sources. In the intracell/network cancellations,  $k$  is approximately 10 and cancellations will start at a half-separation of about 2.5 Mm, so interaction distances greater than 5 Mm will give an X-ray bright point offset from the cancelling magnetic feature. In network/network cancellations, however,  $k$  is approximately

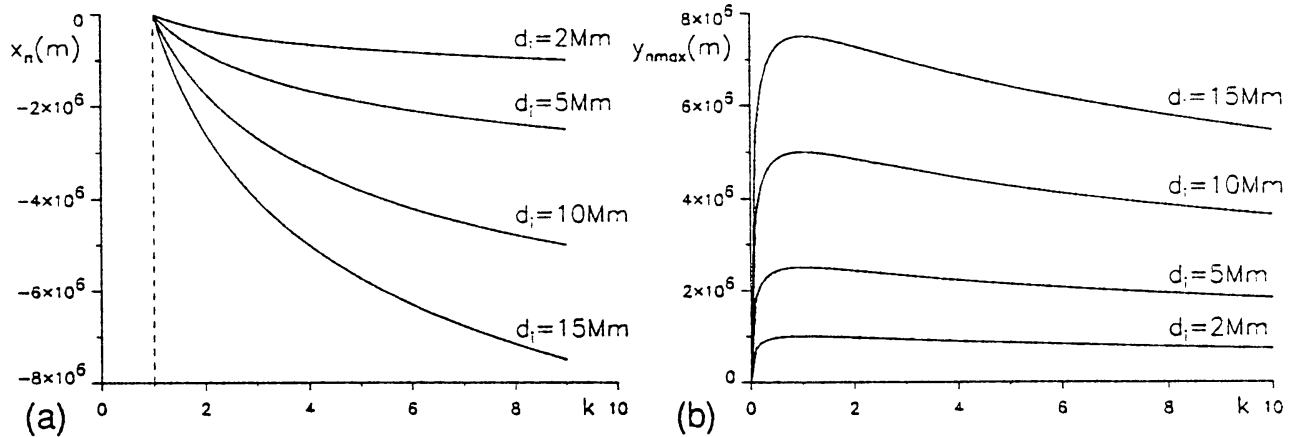


Fig. 4. A graph of the position of the X-type neutral point during the interaction phase versus the pole strength ratio  $k$  for interaction distances  $d_i$  of 2, 5, 10, and 15 Mm. (b) A graph of the maximum height,  $y_{n \max}$ , of the X-type neutral point above the photosphere against  $k$ , for interaction distances  $d_i$  of 2, 5, 10, and 15 Mm.

2 and the cancellation will start at about 5 Mm, so the X-ray bright point is likely to be directly above the cancelling magnetic feature. From Figure 4(b) the height of the X-type neutral point decreases with  $k$  and  $d_i$ , and therefore network/network cancellations will produce bright points higher in the corona than intracell/network cancellations.

### 3. Energy Release

#### 3.1. FORMATION OF A CURRENT SHEET

An estimation for the energy release may be obtained by first supposing that reconnection is not allowed to take place, so that when the poles reach the half-separation distance  $d_i$  a current sheet will start to form and grow as the poles continue moving together. It will extend up from the photosphere from a point  $(x_1, 0)$  to a point  $(x_2, y_2)$ , say. The form for the magnetic field, given as a complex function, is

$$\mathcal{B}(z) = B_y(x, y) + iB_x(x, y) = \frac{iE(z - x_1) \left( (z - x_2)^2 + y_2^2 \right)^{1/2}}{z^2 - a^2}, \quad (12)$$

where  $E$  is a constant and  $a$  is the half-separation as before. The following boundary conditions are found by considering the asymptotic behaviour of the magnetic field:

(i) At large distances the magnetic field must tend to that of the overlying uniform field in the same way as the potential field,  $\mathcal{B}_p(z)$ , so that as

$$z \rightarrow \infty, \quad \mathcal{B}_p(z) \rightarrow \mathcal{B}(z) \rightarrow iB_0.$$

(ii) Near  $z = a$  the magnetic field behaves like a source of strength  $f$ , and so as

$$z \rightarrow a, \quad \mathcal{B} \rightarrow if/(\pi(z-a)).$$

(iii) Similarly near  $z = -a$  the magnetic field behaves like a sink of strength  $-g$ , so as

$$z \rightarrow -a, \quad \mathcal{B} \rightarrow -ig/(\pi(z+a)).$$

After expanding the expressions for  $\mathcal{B}(z)$  and  $\mathcal{B}_p(z)$  the first boundary condition gives

$$iE \left( 1 - \frac{x_1}{z} - \frac{x_2}{z} \right) = iB_0 + \frac{if/\pi}{z} - \frac{ig/\pi}{z} + O\left(\frac{1}{z^2}\right).$$

Thus equating terms of order unity and  $z^{-1}$  we find

$$E = B_0 \tag{13}$$

and

$$x_1 + x_2 = -(f' - g'). \tag{14}$$

The next two conditions give, respectively,

$$f' = \frac{1}{2a}(a - x_1) ((a - x_2)^2 + y_2^2)^{1/2}, \tag{15}$$

$$g' = \frac{1}{2a}(a + x_1) ((a + x_2)^2 + y_2^2)^{1/2}. \tag{16}$$

These two equations can be solved to give  $x_2$  and  $y_2$  in terms of  $x_1$ ,

$$x_2 = -a \left( \frac{f'^2}{(a - x_1)^2} - \frac{g'^2}{(a + x_1)^2} \right), \tag{17}$$

$$y_2 = \sqrt{2a^2 \left( \frac{f'^2}{(a - x_1)^2} + \frac{g'^2}{(a + x_1)^2} \right) - a^2 - x_1^2}. \tag{18}$$

Using Equations (14) and (17), an expression in terms of  $x_1$ ,  $a$ ,  $g'$ , and  $f'$  may be found:

$$\left( f' - \frac{af'^2}{(a - x_1)^2} \right) - \left( g' - \frac{ag'^2}{(a + x_1)^2} \right) + x_1 = 0, \tag{19}$$

or, after completing the two squares,

$$\left(\frac{g'}{(a+x_1)} - \frac{(a+x_1)}{2a}\right)^2 - \left(\frac{f'}{(a-x_1)} - \frac{(a-x_1)}{2a}\right)^2 = 0. \quad (20)$$

Then this equation factorises into a quadratic and a cubic for  $x_1$ , namely

$$x_1^2 + (f' - g')x_1 + a(f' + g' - a) = 0, \quad (21)$$

$$F(x_1) \equiv x_1^3 - a(a + g' + f')x_1 + a^2(g' - f') = 0. \quad (22)$$

Solving the quadratic, which is identical to Equation (2) and hence related to the potential state, does not give any real roots in the interval  $0 < a < d_i$ . The cubic,  $F(x_1)$ , must therefore contain the value of  $x_1$  required. First it is ascertained whether the roots of  $F(x_1)$  are real or imaginary. This is done by differentiating Equation (22) with respect to  $x_1$  to discover the values of  $x_1$  for which  $F(x_1)$  has a maximum or minimum:

$$x_{1 \min} = +\sqrt{\frac{a^2 + a(g' + f')}{3}}, \quad (23)$$

$$x_{1 \max} = +\sqrt{\frac{a^2 + a(g' + f')}{3}}. \quad (24)$$

If  $F(x_{1 \min})$  is less than zero there exist three real distinct roots to  $F(x_1) = 0$ , that is if

$$(g' - f') < \frac{2|a + g' + f'|^{3/2}}{3\sqrt{3a}}. \quad (25)$$

This is trivially satisfied if  $f' > g'$ . For  $f' < g'$  the right-hand side of Equation (25) is differentiated with respect to  $a$  to find that the turning point occurs when  $a = (g' + f')/2$ . This gives a minimum, which when substituted back into the right-hand side of (25) gives

$$g' - f' < g' + f'. \quad (26)$$

Thus we have shown that for all positive values of  $g'$  and  $f'$  and  $0 < a < d_i$ ,  $F(x_1) = 0$  has three real and distinct roots.

From Equation (22), expanding about  $-a$  with  $x_1 = -a + \delta$  gives

$$\delta^3 - 3a\delta^2 + (2a^2 - a(g' + f'))\delta + 2a^2g' = 0. \quad (27)$$

Assuming that the roots to this cubic are  $\alpha, \beta, \gamma$ , then

$$-\alpha\beta\gamma = 2a^2g' > 0, \quad (28)$$

which implies that at least one of the roots is negative; moreover either one or all the roots are negative. Equating the coefficients of  $\delta^2$  implies

$$\alpha + \beta + \gamma = 3a \quad (29)$$

so that not all the roots are negative. Therefore at most one root is negative, which implies that one and only one root of Equation (22) is less than  $-a$ .

Similarly expanding about  $a$  by putting  $x_1 = a + \delta$  gives

$$\delta^3 + 3a\delta^2 + (2a^2 - a(g' + f'))\delta - 2a^2g' = 0. \quad (30)$$

Again assuming that the roots to this cubic are  $\alpha, \beta, \gamma$ , we find

$$\alpha\beta\gamma = 2a^2g' > 0. \quad (31)$$

So either one or all the roots are positive. Considering the coefficients of  $\delta^2$  gives

$$\alpha + \beta + \gamma = -3a. \quad (32)$$

Thus not all the roots are positive, so at most one root is positive and hence one and only one root of Equation (22) is greater than  $a$ . The remaining root therefore must lie in the range  $-a < x_1 < a$  which satisfied the frozen in flux condition. So there exists a unique solution satisfying the boundary conditions for the end-point of the current sheet which equals

$$x_1 = \frac{-(S + T)}{2} + \frac{\sqrt{-3}(S - T)}{2}, \quad (33)$$

where  $S^3 = U + \sqrt{U^2 + V^3}$  and  $T^3 = -U + \sqrt{U^2 + V^3}$ , with  $U = a^2(g' - f')/2$  and  $V = -a(a + g' + f')/3$ .

From Equations (33), (17), and (18) the end-points of the current sheet may now be calculated. It is interesting to note that, by using conservation of flux the above boundary conditions can be found instead by solving the appropriate integrals for the flux across  $x = x_1$  for  $0 \leq y < \infty$ , across  $y = 0$  for  $-\infty < x \leq x_1$  and across  $y = 0$  for  $x_1 \leq x < \infty$ , respectively.

The magnetic field due to the current sheet may be drawn (Figure 5) using Equation (12) with  $E = B_0$ ,  $x_1$  given by (33) and solving for  $x_2$  and  $y_2$  from Equations (33), (17), and (18). Figure 6 shows the endpoints of the current sheet plotted in the  $xy$ -plane for the half-separation,  $a$ , between 0.0 and  $d_i$ , where the poles have a strength ratio of  $k = 3$  and lengths are normalized with respect to  $d_i$ . The shape of the current sheet for  $a = 0.02$  is represented by a dashed curve.

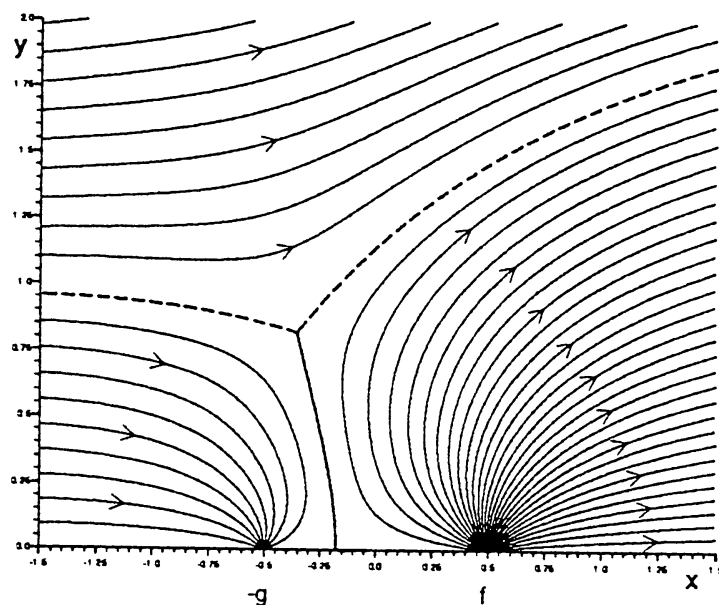


Fig. 5. A plot of the magnetic field with a current sheet according to Equation (12) for a positive pole of strength  $f (= 3g)$  situated at  $z = 0.5$ , a negative pole of strength  $-g = -\pi B_0 / (2 + \sqrt{3})$  situated at  $z = -0.5$  and the background field  $B_0$  of strength 1.0. Lengths have all been normalized with respect to  $d_i$ .

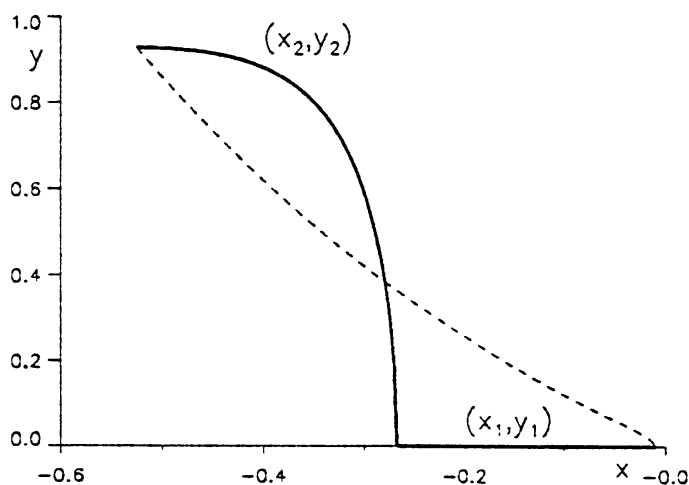


Fig. 6. The positions of the end-points of the current sheet for two poles  $f$  and  $-g$ , where  $f = 3g$ , are plotted in the  $xy$ -plane lying between 0.02 and the interaction distance ( $d_i$ ). The location of the current sheet when  $a = 0.02$  is indicated by a dashed curve.

### 3.2. FREE MAGNETIC ENERGY

The free energy stored in the current sheet can be calculated easily (Hu and Low, 1983; Priest, Parnell, and Martin, 1994) by first considering the total magnetic energy  $W$  in a volume  $V$  with boundary  $S$ ,

$$W = \frac{1}{2\mu} \int_V B^2 dV. \quad (34)$$

Since

$$\mathbf{B} = \nabla \times \mathbf{A}, \quad \mathbf{A} = A \hat{\mathbf{e}}_z,$$

and

$$\nabla \times \mathbf{B} = \mu \mathbf{J}, \quad \mathbf{J} = J \hat{\mathbf{e}}_z,$$

where  $A$  is the flux function and  $J$  is the current density, this may be rewritten with  $d\mathbf{S} = dx \hat{\mathbf{e}}_y$  as

$$W = \frac{1}{2} I_c A_c - \frac{1}{2\mu} \int_{-\infty}^{\infty} (AB_x)_{y=0} dx, \quad (35)$$

where  $I_c$  is the total current flowing in the current sheet and  $A_c$  is the constant value of the vector potential ( $A$ ) at the current sheet which is chosen to be equal to zero for convenience.

Suppose  $\mathbf{B}_p$  is the potential magnetic field with the same normal field on  $y = 0$  as  $\mathbf{B}$ , so that the flux functions for the potential field and the full field are the same at the photosphere ( $A_p = A$  on  $y = 0$ ). Then the magnetic energy of the potential field is

$$W_p = -\frac{1}{2\mu} \int_{-\infty}^{\infty} (AB_{px})_{y=0} dx. \quad (36)$$

The free energy stored in the current sheet is the difference between the total magnetic energy and the energy of the potential field and thus becomes in our two-dimensional field of depth  $d_i$

$$\frac{W_f}{d_i} = \frac{-1}{2\mu} \int_{-\infty}^{\infty} [A(B_x - B_{px})]_{y=0} dx, \quad (37)$$

where  $B_x$ ,  $B_{px}$ , and  $A$  along  $y = 0$  are found to be

$$B_x = \text{Im}[\mathcal{B}(x)] = \frac{B_0(x - x_1) ((x - x_2)^2 + y_2^2)^{1/2}}{x^2 - a^2}. \quad (38)$$

$$B_{px} = \text{Im}[\mathcal{B}_p(x)] = B_0 + \frac{f}{\pi(x - a)} - \frac{g}{\pi(x + a)}, \quad (39)$$

$$A = \left\{ \begin{array}{ll} -\pi B_0 g' (= -g) & -a < x \\ 0 & -a < x < a \\ -\pi B_0 f' (= -f) & x > a \end{array} \right\}. \quad (40)$$

So the free energy stored in the current sheet can be written as

$$\frac{W_f}{d_i} = \frac{-1}{2\mu} \int_{-\infty}^{-a} -g[B_x - B_{px}]_{y=0} dx + \frac{-1}{2\mu} \int_a^{\infty} -f[B_x - B_{px}]_{y=0} dx . \quad (41)$$

This can be solved analytically, by first solving the indefinite integrals

$$\begin{aligned} \int B_{px}|_{y=0} dx &= \int B_0 + \frac{f}{\pi(x-a)} - \frac{g}{\pi(x+a)} dx = \\ &= B_0 \{x + f' \log[x-a] - g' \log[x+a]\} , \end{aligned} \quad (42)$$

$$\int B_x|_{y=0} dx = \int \frac{B_0(x-x_1)((x-x_2)^2 + y_2^2)^{1/2}}{x^2 - a^2} dx , \quad (43)$$

which can be written as

$$\int B_x|_{y=0} dx = \frac{B_0(a-x_1)}{2a} \int \frac{Q(x)}{x-a} dx + \frac{B_0(a+x_1)}{2a} \int \frac{Q(x)}{x+a} dx , \quad (44)$$

where  $Q(x) = ((x-x_2)^2 + y_2^2)^{1/2}$ .

It is noted that

$$Q^2(x) = (x-a)^2 + 2(a-x_2)(x-a) + Q^2(a) , \quad (45)$$

$$Q^2(x) = (x+a)^2 - 2(a+x_2)(x+a) + Q^2(-a) , \quad (46)$$

then

$$\int \frac{Q(x)}{x-a} dx = Q(x) + (a-x_2) \int \frac{dx}{Q(x)} + Q^2(a) \int \frac{dx}{(x-a)Q(x)} , \quad (47)$$

$$\int \frac{Q(x)}{x+a} dx = Q(x) - (a+x_2) \int \frac{dx}{Q(x)} + Q^2(-a) \int \frac{dx}{(x+a)Q(x)} . \quad (48)$$

So Equation (44) becomes

$$\begin{aligned} \int B_x|_{y=0} dx &= B_0 \left\{ Q(x) - (x_1+x_2) \int \frac{dx}{Q(x)} + \frac{(a-x_1)Q^2(a)}{2a} \times \right. \\ &\quad \left. \times \int \frac{dx}{(x-a)Q(x)} + \frac{(a+x_1)Q^2(-a)}{2a} \int \frac{dx}{(x+a)Q(x)} \right\} . \end{aligned} \quad (49)$$

The remaining three integrals can easily be solved to give

$$\int \frac{dx}{Q(x)} = \log[Q(x) + x - x_2] , \quad (50)$$

$$\int \frac{dx}{(x-a)Q(x)} = \frac{-1}{|Q(a)|} \log \left[ \frac{Q^2(a) + (a-x_2)(x-a) + |Q(a)|Q(x)}{x-a} \right], \quad (51)$$

$$\int \frac{dx}{(x+a)Q(x)} = \frac{-1}{|Q(-a)|} \times \log \left[ \frac{Q^2(-a) - (a+x_2)(x+a) + |Q(-a)|Q(x)}{x+a} \right]. \quad (52)$$

Using Equations (14), (15), and (16) the final expression for Equation (43) is

$$\int B_x|_{y=0} dx = B_0 \left\{ Q(x) + (f' - g') \log[Q(x) + x - x_2] - f' \log \left[ \frac{Q^2(a) + (a-x_2)(x-a) + |Q(a)|Q(x)}{x-a} \right] - g' \log \left[ \frac{Q^2(-a) - (a+x_2)(x+a) + |Q(-a)|Q(x)}{x+a} \right] \right\}. \quad (53)$$

Now putting in the limits for the first integral from  $-\infty$  to  $-a$ , and noting that  $Q(x) = -|Q(x)|$ , gives

$$\begin{aligned} & - \int_{-\infty}^{-a} [B_x - B_{px}]_{y=0} dx = \\ & = B_0 \left\{ -a + |Q(-a)| - x_2 + g' \log \left[ \frac{(|Q(-a)| + a + x_2)^2}{4Q^2(-a)} \right] + \right. \\ & \quad \left. + f' \log \left[ \frac{2(|Q(a)||Q(-a)| + 2a(a-x_2) - Q^2(a))}{(|Q(-a)| + a + x_2)(|Q(a)| + a - x_2)} \right] \right\}. \quad (54) \end{aligned}$$

Similarly, putting in the limits for the integral from  $a$  to  $\infty$ , where this time  $Q(x) = |Q(x)|$ , gives

$$\begin{aligned} & - \int_a^{\infty} [B_x - B_{px}]_{y=0} dx = \\ & = B_0 \left\{ -a + |Q(a)| + x_2 + f' \log \left[ \frac{(|Q(a)| + a - x_2)^2}{4Q^2(a)} \right] + \right. \end{aligned}$$

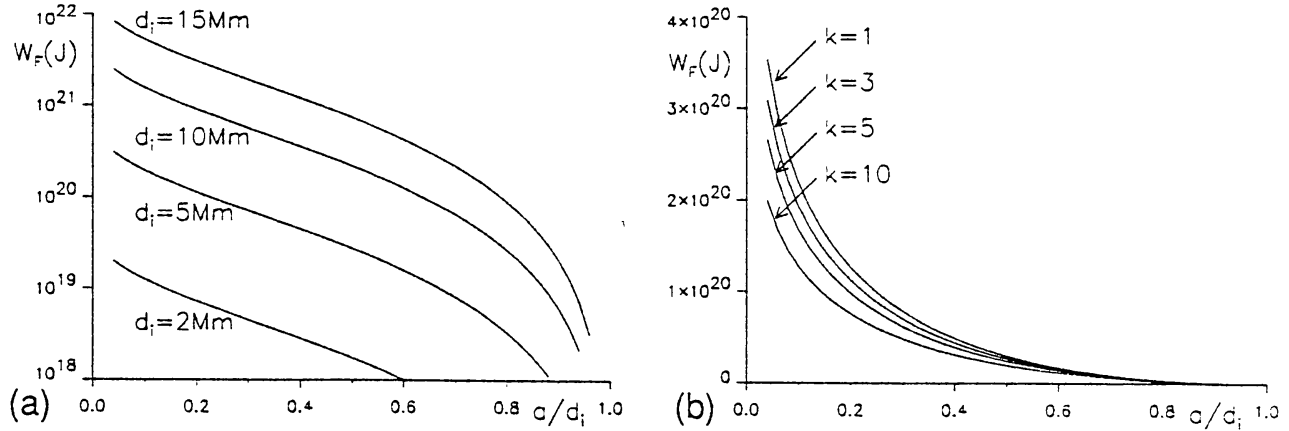


Fig. 7. The free energy ( $W_f$ ) in joules as a function of  $a/d_i$  when the background field  $B_0$  is 10 G for (a) different values of the interaction distance,  $d_i$ , when the pole strength ratio  $k = 3$ , and for (b) different values of  $k$ , the ratio of the pole strengths, with  $d_i = 5$  Mm.

$$+g' \log \left[ \frac{8a^2(|Q(-a)| - a - x_2)}{(Q^2(-a) - 2a(a + x_2) + |Q(a)||Q(-a)|)(|Q(a)| + a - x_2)} \right] \Bigg\}. \quad (55)$$

Thus the free energy stored in the current sheet is finally

$$\begin{aligned} W_f &= \frac{-d_i}{2\mu} \int_{-\infty}^{-a} -g[B_x - B_{px}]_{y=0} dx + \frac{-d_i}{2\mu} \int_a^{\infty} -f[B_x - B_{px}]_{y=0} dx = \\ &= \frac{d_i \pi B_0^2}{2\mu} \left\{ -g'(|Q(-a)| - a - x_2) - f'(|Q(a)| - a + x_2) - \right. \\ &\quad \left. -g'^2 \log \left[ \frac{(|Q(-a)| + a + x_2)^2}{4Q^2(-a)} \right] - f'^2 \log \left[ \frac{(|Q(a)| + a - x_2)^2}{4Q^2(a)} \right] - \right. \\ &\quad \left. -f'g' \log \left[ \frac{4(|Q(a)||Q(-a)| + 2a(a - x_2) - Q^2(a))^2}{(|Q(-a)| + a + x_2)^2 (|Q(a)| + a - x_2)^2} \right] \right\}. \quad (56) \end{aligned}$$

The free magnetic energy stored in the current sheet is plotted in Figure 7(a) on a logarithmic scale as a function of  $a/d_i$  for interaction distances,  $d_i = 2, 5, 10$ , and 15 Mm, with a background field strength  $B_0 = 10$  G, where the pole strengths are  $f' = 3g'$ ,  $g' = d_i/(2 + \sqrt{3})$ . Figure 7(b) shows the free magnetic energy versus  $a/d_i$  for different pole strength ratios,  $k = 1, 3, 5$ , and 10, where the interaction distance is 5 Mm and the ambient field,  $B_0$ , is 10 G. An average X-ray bright point with a lifetime of 8 hours emits a total energy of  $3 \times 10^{20} - 3 \times 10^{21}$  J, which correspond to the energies attained in Figure 7(a) for interaction distances from 5–10 Mm and for pole strength ratios of 1–3 in Figure 7(b).

#### 4. Conclusion

The development here of the converging flux model of Priest, Parnell, and Martin (1994) for the interaction of two magnetic sources of opposite sign and differing strengths agrees with many key X-ray bright point and cancelling magnetic feature observations. The pre-interaction phase shows unconnected sources suggesting no chromospheric fibrils linking the magnetic fragments. It creates an X-ray bright point in the interaction phase due to reconnection in the corona. This bright point is shown to lie near the cancelling magnetic feature but not necessarily directly above it. Then cancellation of the magnetic fragments occurs by reconnection in the photosphere. A new phase is found to start at the end of the interaction phase, called the capture phase, where the weaker pole is fully connected to the stronger pole as the poles continue to converge.

With the added variation in the ratio of the pole strengths, the complete range of bright-point lifetimes may be explained and we suggest that it would be useful in future observational studies to compare the bright-point properties with the ratio of the source strengths. For example, the model suggests that two poles of similar strengths ( $k \approx 1$ ) and a large interaction distance would give a long bright-point lifetime, as in network/network cancellations, whereas in intracell/network cancellations where  $k = 10$ , say, and  $d_i = 2-5$  Mm the bright point would only last a few hours. We suggest from our model that not all types of cancelling magnetic feature will have capture phase, but such a phase is more likely to occur in intracell/network cancellations. This means that in this type of cancelling magnetic feature the X-ray bright point would be expected to start well before the cancellation, and may even have finished before the fragments start cancelling. In a network/network cancellation the cancelling magnetic feature is likely to begin several hours before the bright point ends.

If during the interaction phase reconnection is inhibited from taking place, a current sheet forms. The magnetic field due to this situation has been drawn, as has a graph of the end-points of the current sheet versus the half-separation,  $a$ . The current sheet grows as the half-separation of the poles,  $a$ , becomes smaller. The free energy stored in the current sheet has been calculated giving an estimate of the amount of energy that can be released at any one time during the bright point, and so it would also be interesting to compare the predicted energies with future observations. The variation in the ratio of pole strengths gives a range of total energies released during the bright point. Two poles with a pole ratio of 5, velocity of  $0.15 \text{ km s}^{-1}$  and interaction distance of 5 Mm would create an X-ray bright point with a lifetime of 8 hours and total energy emission of  $3 \times 10^{20}$  J, similar to the observed values for a normal 8-hour bright point of  $3 \times 10^{20} - 3 \times 10^{21}$  J. The model also suggests that bright points are more likely to lie directly above their cancellation sites for network/network cancellations between strong magnetic fragments of similar strengths, whereas bright points may be offset to

one side of the cancelling magnetic fragment when cancellations between magnetic fragments of dissimilar strengths occur, as in intracell/network cancellations.

### Acknowledgements

The authors would like to thank the U.K. Science and Engineering Research Council for their financial support.

### References

- Dere, K. P.: 1993, *Proc. 2nd SOHO Workshop, Elba, ESA*, in press.
- Golub, L., Krieger, A. S., and Vaiana, G. S.: 1976a, *Solar Phys.* **49**, 79.
- Golub, L., Krieger, A. S., and Vaiana, G. S.: 1976b, *Solar Phys.* **50**, 311.
- Golub, L., Krieger, A. S., Silk, J., Timothy, A., and Vaiana, G. S.: 1974, *Astrophys. J.* **189**, L93.
- Golub, L., Krieger, A. S., Harvey, J., and Vaiana, G. S.: 1977, *Solar Phys.* **53**, 111.
- Harvey, K. L.: 1984, *Proc. 4th European Meeting on Solar Physics*, ESA SP 220, p. 235.
- Harvey, K. L.: 1985, *Australian J. Phys.* **38**, 875.
- Hu, Y. Q. and Low, B. C.: 1983, *Solar Phys.* **84**, 83.
- Martin, S. F.: 1984, in S. Keil (ed.), *Small-Scale Dynamical Processes in Stellar Atmospheres*, Sacramento Peak Observatory, p. 30.
- Martin, S. F.: 1986, in A. Poland (ed.), *Coronal and Prominence Plasmas*, NASA CP 2442, p. 431.
- Martin, S. F.: 1988, *Solar Phys.* **117**, 243.
- Martin, S. F., Livi, S. H. B., Wang, J., and Shi, Z.: 1984, in M. Hagyard (ed.), *Measurements of Solar Vector Magnetic Fields*, NASA CP 2374, p. 403.
- Priest, E. R., Parnell, C. E., and Martin, S. F.: 1994, *Astrophys. J.*, in press.
- Shibata, K., Ishido, Y., Acton, L., Strong, K., Hirayama, T., Uchida, Y., McAllister, A., Matsumoto, R., Tsuneta, S., Shimizu, T., Hara, H., Sakurai, T., Ichimoto, K., Nishino, Y., and Ogawara, Y.: 1992, *Publ. Astron. Soc. Japan* **44**, L173.
- Shimizu, T., Tsuneta, S., Acton, L., Lemen, J. R., and Uchida, Y.: 1992, *Publ. Astron. Soc. Japan* **44**, L147.
- Vaiana, G. S., Krieger, A. S., Van Speybroeck, L. P., and Zehnpfennig, T.: 1970, *Bull. Am. Phys. Soc.* **15**, 611.
- Webb, D. F., Martin, S. F., Moses, D., and Harvey, J. W.: 1993, *Solar Phys.* **144**, 15.